Optics Letters

# GaN-based green resonant-cavity light-emitting diodes with Al mirror and copper plate

Shuai Yang,[1] Huan Xu,[1] Hao Long,[1] Leiying Ying,[1] Ronghuang Luo,[2] Mengjie Zhong,[2] Wenrui Lu,[2] Xiang Hou,[2] Yang Mei,[1,3] and Baoping Zhang[1,4]

[1]School of Electronic Science and Engineering, Xiamen University, Xiamen 361005, China
[2]Fujian Zhongjing Technology Co., Ltd., Longyan 361000, China
[3]e-mail: meiyang@xmu.edu.cn
[4]e-mail: bzhang@xmu.edu.cn

Received 10 March 2022; revised 9 May 2022; accepted 9 May 2022; posted 10 May 2022; published 26 May 2022

**In this Letter, GaN-based green resonant-cavity light-emitting diodes (RCLEDs) with a low-cost aluminum (Al) metal bottom mirror, a dielectric top mirror, and a copper (Cu) supporting plate were fabricated. The green-emitting epitaxial wafer was grown on a patterned sapphire substrate (PSS) to ensure high crystal quality (CQ). Laser lift-off (LLO) of the PSS and electrical plating of a Cu supporting plate were then carried out to realize the vertical device structure. The emission wavelength and full width at half maximum (FWHM) of the main emission peak of the device are ~518 nm and 14 nm, respectively. Under the current density of 50 A/cm$^2$, a relatively high light output power (LOP) of 11.1 mW can be obtained from the green RCLED. Moreover, when the current injection is 20 mA (8 A/cm$^2$), the corresponding forward bias voltage is as low as ~2.46 V. The reasons for the low operating voltage and high LOP can be attributed to the improvement of CQ, the release of residual compressive stress of the GaN-based epilayer due to the removal of PSS, and better heat dissipation properties of the Cu supporting plate.** 

https://doi.org/10.1364/OL.458088

GaN-based materials have been attracting a lot of attention in the fabrication of LED and laser diodes because of their environment-friendly, chemically-stable, strong anti-radiation performance. The emission wavelength of GaN-based materials can be tuned over a wide range from the ultraviolet to the visible, which offers an excellent potential substitute for aspects of biological lighting, solid-state lighting, and full-color display [1]. With the rapid development of GaN-based LEDs, GaN-based resonant-cavity light-emitting diodes (RCLEDs) are becoming more attractive because of their pure emission as well as their narrower linewidth, higher brightness and modulation rate, and better thermal stability. In particular, green-emitting RCLEDs are promising in applications such as plastic optical fiber (POF) and underwater wireless communication (UWC) [2].

Up to now, GaN-based green RCLEDs with different cavity mirror designs using a combination of epitaxial nitride-based distributed Bragg reflectors (DBRs), dielectric DBRs, and metal mirrors have been realized by several research groups. In 2002, Maaskant *et al*. reported a GaN-based green RCLED of 490 nm on a sapphire substrate with a 6-period epitaxial bottom AlGaN/GaN DBR and a Pd/Ag top mirror. The forward voltage and light output power (LOP) were 3.5 V at 20 mA and 330 μW, respectively [3]. In the same year, Naranjo *et al*. reported a GaN-based green RCLED with a 7-period epitaxial AlGaN/GaN DBR and an Al mirror as the bottom and top reflectors, respectively. The emission wavelength was ~510 nm and the forward voltage was a relatively large 7 V at 20 mA [4]. In those reports, the growth of AlGaN/GaN DBR with high reflectivity was difficult because of the low index contrast and large lattice mismatch. In 2006, a GaN-based green RCLED on an Si substrate with a combination of a bottom Ag mirror and a top dielectric mirror was reported by Horng *et al*. [5]. The following year they also reported green RCLEDs with double dielectric DBRs on an Si substrate [6]. All the devices above featured a lateral current injection structure, which will cause a current crowding effect. In 2008, Huang *et al*. fabricated a green RCLED with a vertical current injection structure and a copper substrate. A three-pair dielectric $TiO_2/SiO_2$ DBR and a Ti-Al metal mirror were used as the top and bottom reflectors, respectively. The turn-on voltage was 4.2 V at 20 mA and the maximum LOP exceeded 1 mW [7]. More recently, Wu *et al*. reported a vertical green RCLED with trapezoidal quantum wells (QWs). A five-pair dielectric $TiO_2/SiO_2$ DBR and an Ag mirror as top and bottom reflectors, respectively, were used. The highest laser lift-off (LLO) of 115 mW was obtained at 450 mA (210 A/cm$^2$) and the turn-on voltage was 2.95 V [8]. Despite the rapid development of GaN-based green RCLEDs, device performance is still limited, mostly by the poor crystal quality (CQ) of InGaN QWs in the green region, which is mainly due to the low growth temperature and large lattice mismatch between the QW with high indium content and the quantum barrier [9]. The large lattice mismatch between the epitaxy substrate and GaN-based epitaxial layer was also one of the reasons for the worse CQ of epitaxial layers [10]. The high-density defects and dislocations in InGaN green multiple quantum wells (MQWs) can increase the nonradiative recombination for carriers, and further degenerate the electro-optical conversion efficiency. At present, most common methods to improve the emitting efficiency of InGaN green LEDs require using patterned sapphire substrates (PSSs) and inserting superlattices (SLs) beneath the QWs. The PSS can improve the CQ of epitaxial layers with the lateral growth mode, which not only

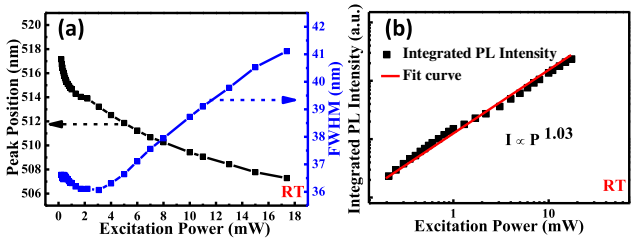


**Fig. 1.** (a) Peak position and FWHM of MQWs as a function of excitation power. (b) Excitation power-dependent integrated PL intensity.

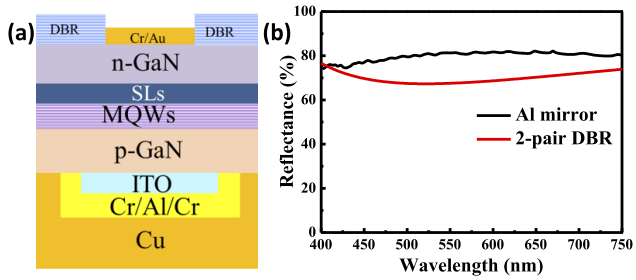


**Fig. 2.** (a) Schematic structure of the RCLED. (b) Reflectivity of the Al mirror and top DBR.

induce strain relaxation but also decrease threading dislocation density [11]. In addition, having SLs beneath the QWs as a strain-relief layer can improve the CQ of MQWs. First, strain relaxation can be achieved by using SLs as an ideal buffer platform. Second, the SLs utilized for the further growth of MQWs can act as a filter of threading dislocations from the GaN buffer layer, further reducing the carrier leakage paths [9]. However, for green RCLEDs, the original substrate for material growth usually needs to be lifted off to form a cavity structure, which is more difficult for PSSs.

In this Letter, green InGaN QWs with high CQ were grown by using PSS and SL inserting layers, and green RCLEDs with a vertical current injection scheme on a Cu plate were successfully fabricated using the LLO technique. The resonant cavity contained a low-cost Al bottom mirror and two pairs of dielectric $TiO_2/SiO_2$ top DBRs and was transferred to a Cu supporting plate to improve the heat dissipation. The devices showed an emission wavelength of 518 nm and a FWHM of 14 nm. The maximum LOP was 11.1 mW when the current density was about 50 A/cm$^2$. Moreover, the turn-on voltage was very low ~ 2.46 V at 20 mA. This successful fabrication of green vertical RCLEDs will facilitate the rapid development of high-performance GaN-based green devices.

The GaN-based epitaxial layers were grown on the c-plane (0001) PSS via the metal-organic chemical vapor deposition (MOCVD) system. The epitaxy structure and power-dependent photoluminescence (PL) spectra are shown in Supplement 1 (Fig. S1). The active region contains 10 pairs $In_{0.25}Ga_{0.75}N$/GaN (3 /12.6 nm) MQWs, and 30 pairs low In content $In_{0.05}GaN_{0.95}$/GaN (1 /2 nm) SLs were grown first before the active region to release the strain and enhance indium incorporation of the MQWs. Figure 1(a) shows the excitation power-dependent PL peak position and FWHM of green InGaN/GaN MQWs. The PL peak position exhibits a blueshift from 517.4 nm to 507 nm with the increase of excitation power. This slight blueshift can be attributed to the screening of quantum-confined Stark effect (QCSE) resulting from the piezoelectric field in the MQWs [12]. The FWHM first decreased slightly from 36.6 nm to 36 nm and then increased from 36 nm to 41.1 nm. The variation of FWHM and the monotonous blueshift of PL peak position for MQWs are mainly ascribed to the combination of the Coulomb screening of QCSE and the band-filling effect. But the relatively small value of the ~10 nm blueshift and ~5 nm spectral broadening [13] reflect both the weaker polarization field and the better CQ of the MQWs layers based on SL insertion layers and PSS in this Letter [11]. The epi-wafer in this Letter also shows a high IQE of 65% when compared with that grown on a flat sapphire substrate (see Supplement 1, Fig. S3).

The high CQ of the epitaxial layers can also be demonstrated by the evolution of integrated PL intensity with excitation power, as shown in Fig. 1(b). Generally, the integrated PL intensity (I) is proportional to the excitation power (P) [14]:

$$I \propto P^f, \tag{1}$$

where the excitation power index (f) represents the different recombination processes for carriers in the MQWs. If f is equal to 1, it can be inferred that carrier combination processes in the MQWs are mainly radiative recombination. Otherwise, the non-radiative recombination processes dominate for the carriers in the MQWs [15]. The experimentally obtained f value of 1.03 is approaching 1 in this Letter, which means that radiative recombination dominates the recombination process for carriers in the MQWs.

The 4-inch epi-wafer was sliced into 2 cm×2 cm pieces for device fabrication. The device in this Letter features an Al bottom mirror and a dielectric top DBR, and a Cu plate was electroplated to improve thermal dissipation, as illustrated by the device structure in Fig. 2(a). To fabricate the device, 60 nm of indium-tin-oxide (ITO) was deposited on the p-side GaN as the current-spreading layer. An Al mirror consisting of Cr/Al/Cr (1 nm/250 nm/20 nm) layers was then deposited on the ITO. After that, a thick Cu plate (~150 μm) with high thermal and electrical conductivity was electroplated on the surface as a permanent supporting substrate. The PSS was removed using the LLO technique which employed a KrF pulsed excimer laser with a 248 nm wavelength and 20 ns pulse width. The energy density on the surface of the sample is ~69.7 mJ/mm$^2$. The surface of n-GaN was then flatted by a chemico-mechanical polishing (CMP) process, and the period patterns caused by PSS successfully removed, inducing an atomic-level flat surface with 8×8 μm$^2$ root mean square (RMS) roughness of 0.28 nm (see Supplement 1, Fig. S4).

Then, the devices with 500×500 μm$^2$ square mesas were separated by inductively coupled plasma (ICP) etching. Eventually, a two-pair $TiO_2$-$SiO_2$ dielectric DBR and top electrode were deposited. The reflectivity of the top dielectric DBR and bottom metal mirror in this study was measured by ultraviolet–visible–near-infrared (UV–Vis–NIR) spectroscopy (UV-3600), as shown in Fig. 2(b). The Al mirror and top DBR show a reflectivity exceeding 80% and 65% in the 500 nm to ~700 nm wavelength region, respectively.

To clarify the effect of LLO on the emission properties of the MQWs, the PL spectra were measured before and after LLO of the PSS. Here, the original epitaxial wafer is defined as W1, and the sample after the LLO and CMP processes is defined as S1. The normalized PL spectra of the two samples under the same

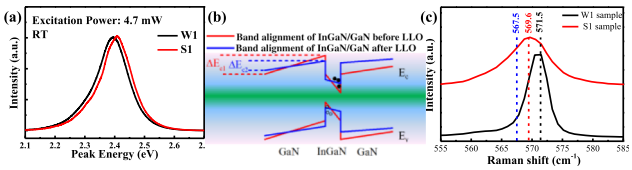


**Fig. 3.** (a) PL spectra of the samples W1 and S1. (b) Schematic diagram of the band alignment of InGaN/GaN before and after LLO. (c) Raman spectra for S1 and W1 samples.

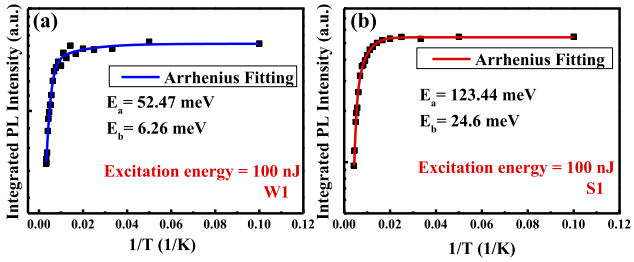


**Fig. 4.** Arrhenius plots of the integral PL intensity dependence on temperature of (a) samples W1, and (b) samples S1.

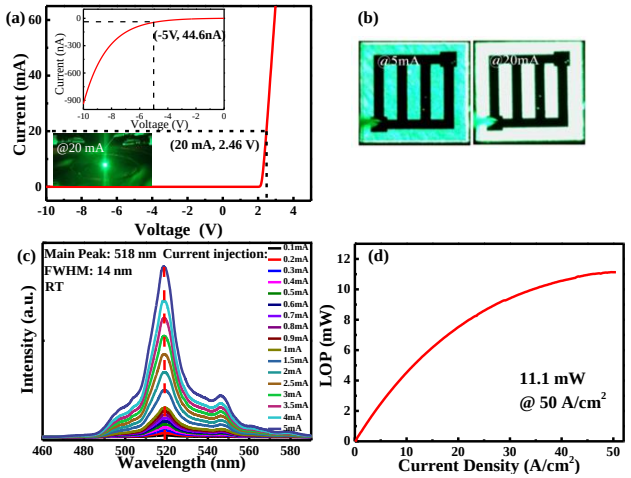


**Fig. 5.** (a) I–V characteristic of the RCLED. Inset: the enlargement diagram of the current versus bias voltage and the photo of luminescence at 20 mA. (b) Microscope images of the RCLED at driving currents of 5 and 20 mA. (c) EL spectra as a function of the different current injection of the RCLED. (d) Curve of the current density versus LOP of the RCLED.

excitation power are displayed in Fig. 3(a). The peak energy of S1 (2.41 eV) shifted to a higher energy compared with that of W1 (2.39 eV). The possibility that the blueshift is caused by the inhomogeneous emission wavelength of the epi-wafer can be excluded (see Supplement 1, Fig. S2). The reason for the obvious blueshift can be attributed to the removal of the PSS of the sample, which results in the release of compressive stress in the GaN template and MQWs. Usually, the GaN grown on a sapphire substrate is under compressive strain, and the residual stress will further increase the lattice mismatch between the GaN template and InGaN QWs, inducing higher QCSE. When the sapphire is lifted off, the residual compressive stress is reduced, and the QCSE and band bending can be weakened, inducing the blueshift of the PL spectrum. The partially released compressive stress can also reduce the potential barrier ($\Delta E_c$) for GaN layers [12]. As schematically shown in Fig. 3(b), the $\Delta E_{c1}$ of W1 can be larger than $\Delta E_{c2}$ of S1. This means that more carriers can be injected into the QW of InGaN/GaN MQWs under the same current injection conditions [16], which is beneficial for the improvement of the optoelectronic properties of the device.

To further verify the release of compressive stress, Raman spectroscopy is conducted before and after LLO, as shown in Fig. 3(c). The GaN $E_2$ (high) peak (569.6 $cm^{-1}$) of S1 is evidently shifted to a lower wavenumber than W1 (571.5 $cm^{-1}$). The slight left shift of the $E_2$ (high) peak of S1 represents an increase of GaN lattice constant, and the residual compressive stress in W1 and S1 is calculated to be 0.93 and 0.49 GPa [17], respectively, when compared with the $E_2$ (high) peak for the free-standing GaN of 567.5 $cm^{-1}$ [18], further proving the release of compressive stress. This is consistent with the blueshift of the PL spectrum.

The temperature-dependent PL characteristics were also measured for W1 and S1 from 3 K to 300 K, as shown in Fig. 4. The activation energy of nonradiative recombination centers of W1 and S1 were calculated and fitted by the Arrhenius function [19]:

$$I(T) = \frac{1}{1 + \sum_i C_i \exp\left(-\frac{E_i}{k_B T}\right)}, \quad (2)$$

where $E_i$ is the activation energy of corresponding nonradiative recombination centers, $C_i$ is the constant related to the density of nonradiative recombination centers, and $k_B$ is the Boltzmann constant. The solid lines in Fig. 4 are the fitting curves of samples by supposing two nonradiative channels. It was identified that the $E_a$ and $E_b$ values of sample S1 were 123.44 and 24.6 meV, respectively, which were larger than those of W1. These results indicated that, compared with sample W1, carriers of sample S1 were more difficult to capture by the nonradiative recombination centers. In other words, more carriers can participate in the radiative recombination process, resulting in the increase of luminescence efficiency and further improvement of the LOP of the devices.

The optoelectronic properties of GaN-based green RCLEDs were performed under RT and CW operation. Figure 5(a) shows the current-voltage (I-V) characteristics and a photo of the device which had a relatively low reverse leakage current of ~44.6 nA when the reverse bias voltage was –5 V. This might be attributed to the high-quality epitaxial layers and the reduction of the leakage current channels owing to the decrease in the number of defects. Meanwhile, a very low turn-on voltage of 2.46 V at 20 mA was realized. This could be due to the decrease in the tilt of the energy band and potential barrier of GaN film, which resulted in the transportation of more carriers reaching the MQWs under the relatively lower forward voltage. Furthermore, high-quality epitaxial films with fewer structural defects obtained by using PSS can also contribute to the lower turn-on voltage. Moreover, SL insertion layers were introduced into epitaxial layers so that the carrier injection of the n-GaN side could be uniformly injected into MQWs, further resulting in a decrease in turn-on voltage [9].

Figure 5(b) shows the light-emitting patterns of the green RCLED under different current injection at 5 and 20 mA, from which the uniform green light of the device can be observed. As seen in Fig. 5(c), the EL intensity of the device becomes stronger with increasing driving currents from 0.1 mA to 5 mA. Three

peaks were clearly observed at 497 nm, 518 nm, and 545 nm, which could be due to the resonant-cavity effect of Fabry–Perot (F–P). To confirm the cavity effect, the cavity modes were simulated by the simple F–P cavity model, correlating well with the emission peaks (see Supplement 1, Fig. S5), and the main peak at 518 nm has a FWHM of ~14 nm at 2 A/cm$^2$, much smaller than that of a vertical LED without cavity (see Supplement 1, Fig. S6).

The LOP of the device was measured by an integrating sphere system and is shown in Fig. 5(d). The LOP of the device was 11.1 mW at 50 A/cm$^2$, which is the highest LOP value for the GaN-based green RCLED with Al mirror [4,7] (see Supplement 1, Table S1). The higher LOP benefits from the improved CQ of the MQWs owing to the PSS and SL insertion layers. In addition, for S1 in which the PSS was removed, the overlap of electron-hole wave functions can be enhanced, and the carriers flowed more easily across the barriers due to the alleviation of the QCSE, which led to higher luminescence efficiency. In addition, the nonradiative recombination activation energy $E_a$ of sample S1 was larger than W1, and it is more difficult for the charged carriers in MQWs to escape from the deep localization states. Effective heat dissipation by the copper plate can also improve the device performance [20]. Based upon these conditions, we fabricated a GaN-based green vertical RCLED device with a relatively high LOP. The LOP in this study is smaller than the record value of 115 mW reported in Ref. [8], Wu *et al* where the noble metal Ag was used as the bottom mirror, which will increase the cost of device fabrication. The LOP in this Letter is expected to be further improved by optimizing the growth conditions in the future work.

In summary, we have fabricated GaN-based green RCLEDs by using epitaxial wafers grown on PSS and other techniques such as LLO, electrical plating, etc. The high-quality material of the MQW active region is fabricated by inserting the PSS and SL layer. The PL characteristics of the MQWs before and after the LLO process were systematically studied and the electroplated Cu supporting plate could improve the heat dissipation for the device. Finally, the GaN-based green RCLED with an emission wavelength of 518 nm and FWHM of 14 nm can be fabricated. The devices feature a low turn-on voltage of 2.46 V at 20 mA and a high LOP of 11.1 mW at 50 A/cm$^2$.

**Funding.** National Natural Science Foundation of China (62104204, U21A20493); National Key Research and Development Program of China (2017YFE0131500).

**Disclosures.** The authors declare no conflicts of interest.

**Data availability.** Data underlying the results presented in this Letter are not publicly available at this time but may be obtained from the authors upon reasonable request.

**Supplemental document.** See Supplement 1 for supporting content.

## REFERENCES

1. C. F. Huang, C. F. Lu, T. Y. Tang, J. J. Huang, and C. C. Yang, Appl. Phys. Lett. **90**, 151122 (2007).
2. E. F. Schubert, N. Hunt, R. J. Malik, M. Micovic, and D. L. Miller, J. Lightwave Technol. **14**, 1721 (1996).
3. P. Maaskant, M. Akhter, B. Roycroft, E. O'Carroll, and B. Corbett, phys. status solidi (a) **192**, 348 (2002).
4. F. Naranjo, S. Fernandez, F. Calle, M. Sánchez-García, and E. Calleja, phys. status solidi (a) **192**, 341 (2002).
5. R. H. Horng, W. K. Wang, S. Y. Huang, and D. S. Wuu, IEEE Photon. Technol. Lett. **18**, 457 (2006).
6. S. Y. Huang, R. H. Horng, D. S. Wuu, W. K. Wang, T. E. Yu, P. R. Lin, and F. S. Juang, Jpn. J. Appl. Phys. **46**, 3416 (2007).
7. S. Y. Huang, R. H. Horng, P. L. Liu, J. Y. Wu, H. W. Wu, and D. S. Wuu, IEEE Photon. Technol. Lett. **20**, 797 (2008).
8. H. Wu, H. Li, S. Y. Kuo, B. Y. Chen, T. C. Lu, and H. Huang, IEEE Trans. Electron Devices. **67**, 3650 (2020).
9. X. Yang, J. Zhang, X. Wang, C. Zheng, Z. Quan, and F. Jiang, Superlattice. Microst. **141**, 106459 (2020).
10. D. M. Graham, A. Soltani-Vala, P. Dawson, M. J. Godfrey, T. M. Smeeton, J. S. Barnard, M. J. Kappers, C. J. Humphreys, and E. J. Thrush, J. Appl. Phys. **97**, 103508 (2005).
11. X. J. Pei, L. W. Guo, X. H. Wang, Y. Wang, H. Q. Jia, H. Chen, and J. M. Zhou, Chinese Phys. Lett. **26**, 028101 (2009).
12. M. H. Doan, S. Kim, J. J. Lee, H. Lim, F. Rotermund, and K. Kim, AIP Adv. **2**, 022122 (2012).
13. Q. Wang, Z. W. Ji, F. Wang, Q. Mu, Y. J. Zheng, X. G. Xu, Y. J. Lü, and Z. H. Feng, Chin. Phys. B **24**, 024219 (2015).
14. R. B. Xu, H. Xu, Y. Mei, X. L. Shi, and H. C. Kuo, J. Lumin. **216**, 116717 (2019).
15. H. L. Ozgur, X. Li, X. Ni, and H. Morkoc, Proc. IEEE **98**, 1180 (2010).
16. R. Sharma, P. M. Pattison, H. Masui, R. M. Farrell, T. J. Baker, B. A. Haskell, F. Wu, S. P. DenBaars, J. S. Speck, and S. Nakamura, Appl. Phys. Lett. **87**, 231110 (2005).
17. W. Wang, Y. Li, Y. Zheng, Z. Yang, Z. Lin, X. Chen, Z. Lu, and G. Li, Cryst. Eng. Comm. **20**, 4685 (2018).
18. Y. Li, W. Wang, X. Li, L. Huang, Z. Lin, Y. Zheng, X. Chen, and G. Li, J. Alloy. Compd. **771**, 1000 (2019).
19. T. Li, A. M. Fischer, Q. Y. Wei, F. A. Ponce, T. Detchprohm, and C. Wetzel, Appl. Phys. Lett. **96**, 031906 (2010).
20. W. S. Wong, A. B. Wengrow, Y. Cho, A. Salleo, N. J. Quitoriano, N. W. Cheung, and T. Sands, J. Electron. Mater. **28**, 1409 (1999).